applied sciences

MDPI

Article

Computational Fluid Dynamics Investigation of Hydrodynamic Forces and Moments Acting on Stern Rudder Plane Configurations of a Submarine

Thanh Long Phan [1], Thi Loan Mai [2] and Tien Thua Nguyen [1,*]

[1] Department of Transportation Mechanical Engineering, The University of Danang—University of Science and Technology, Da Nang 50000, Vietnam; ptlong@dut.udn.vn
[2] Department of Naval Architecture and Marine Engineering, Changwon National University, Gyeongnam 51140, Republic of Korea; mailoankttt@gmail.com
* Correspondence: ntthua@dut.udn.vn

Abstract: This study presents the predicted hydrodynamic characteristics of different rudder plane configurations on the stern of a full-scale submarine in deep water, which are obtained using the Reynolds-Averaged Navier–Stokes method in Ansys Fluent Solver. First, the results obtained for the X-rudder plane configuration are verified according to previous numerical and experimental results in order to assess the accuracy of the simulation procedure. The X-rudder plane, Y-rudder plane, and Cross-rudder plane configurations in deep water with deflection angles ranging from −21 degrees to +21 degrees are then simulated. Next, the hydrodynamic forces and moments of the Cross-plane, X-plane, and Y-plane rudder configurations obtained through simulation are analyzed using Taylor's expansion to estimate the hydrodynamic coefficients. The obtained results demonstrate that the X-force of the X-plane rudder configuration is larger than the corresponding forces acting on the Cross-plane rudder and Y-plane rudder configurations. Meanwhile, the Y-force and Z-force of the X-plane rudder configuration are significantly greater than the corresponding forces of the left configurations. The same tendency can be seen in the moment of the X-plane rudder about the *y*- and *z*-axes. However, the roll moment induced by the Y-plane and Cross-plane rudder configurations is significantly larger than that under the X-plane rudder configuration.

Keywords: submarine; stern rudder plane configuration; rudder force and moment; RANS-based simulation

Citation: Phan, T.L.; Mai, T.L.; Nguyen, T.T. Computational Fluid Dynamics Investigation of Hydrodynamic Forces and Moments Acting on Stern Rudder Plane Configurations of a Submarine. *Appl. Sci.* **2024**, *14*, 4292. https://doi.org/10.3390/app14104292

Received: 2 April 2024
Revised: 7 May 2024
Accepted: 9 May 2024
Published: 18 May 2024

1. Introduction

The maneuvering characteristics are some of the most important performance indicators of marine vehicles such as submarines. The rudder-plane configuration has a significant impact on controlling a ship's journey and, hence, the hydrodynamic forces and moments under different rudder plane configurations are needed for relevant analyses. Three types of rudder-plane configurations are often equipped on submarines; namely, Cross-plane, X-plane, and Y-plane rudders. Experimental studies on submarines appended with a control surface and/or marine propeller are frequently conducted, such as those detailed in [1–5]. For example, research on the prediction of hydrodynamic coefficients of rudders, stabilizers, and the submarine body has been presented by Park et al. [1]. The obtained results showed that the control forces of stabilizers and rudders have a linear variation in the range of deflection angle from −10 to +10 degrees. Experiments on both rudders and stabilizers were carried out in a towing tank with the deflection angle ranging from −30 degrees to +30 degrees. In addition, using an experimental method, Ke et al. [2] predicted the lateral force and yaw moment under the Cross-skeg rudder and X-rudder configurations. The axial velocities of fluid flow induced by the rudder plane configurations were investigated. The stern of the SUBOFF-G submarine with a propeller

and the Cross-rudder plane configuration was automatic maneuvered to carry out the forward running and diving motions. Moreover, the hydrodynamic force and moment of the cruciform stern configuration and the X-rudder plane configuration located at stern of an AUV have been predicted by Kim et al. [3], using both an experimental method and a CFD-based approach. It was shown that the hydrodynamic coefficients of the cruciform stern configuration obtained from the numerical results are in good agreement with the experimental results; however, the differences between the CFD results and experimental results under the X-rudder plane configuration were 43.8% and 53.2% for the hydrodynamic coefficients of the normal force and torque, respectively. An experiment considering a submarine model in the Low-Speed Tunnel has been conducted to measure the cross-stream and in-plane velocities [4], and the experimental results were used for comparison with the CFD-based results for a submarine appended with rudders and stabilizers. On the other hand, measurement of the velocity in the stern wake of a SUBOFF submarine at a high angle of attack has been performed [5], and the axial velocity, tangential velocity, and vorticity were measured and presented in a rectangular domain to analyze the variation of fluid flow induced by the submarine body and the Cross-rudder plane configuration. Although the experimental methods are accurate for determining the hydrodynamic forces and moments of submarines with the stern rudder plane configuration, they also have disadvantages such as the limitations imposed by the water tank, measurement devices, and noise.

Computational Fluid Dynamics (CFD) methods have been widely used for the prediction of hydrodynamics acting on marine vehicles, due to their various advantages. Each type of the rudder-plane configuration had been applied to predict the maneuvering characteristics of the submerged body as shown in [4,6–10]. The straight ahead motion and side-slip motion at 10 degrees of a model of the DSTO generic submarine with full appendages have been investigated using the RANS (Reynolds-averaged Navier–stokes) and LES (Large Eddy Simulation) methods [4]. The fluid flow characteristics obtained from the numerical simulation, such as axial velocity profiles, displacement of vortex core, and turbulent intensity, were compared with the experimental results. Nguyen [6] performed numerical analysis of a full-scale submarine with Cross-rudder plane configuration based on Ansys Fluent code. The hydrodynamic forces and moment of the hull and asymmetric rudders and stabilizers were predicted. In addition, CFD-based simulation of the BB2 submarine has been performed by Cho et al. [7], in order to predict the hydrodynamic forces and moments acting on the hull and X-rudder plane configuration. Hydrodynamic forces, moments, and added masses of the submarine hull were obtained to evaluate the maneuvering characteristics of the submarine with six degrees of freedom; the thrust and moment of the propeller were estimated in open water conditions; and the turning ability of the submarine was verified according to the results obtained from free-running model tests. The normal force and yaw moment caused by rudders and stabilizers in the X-rudder plane configuration varied linearly over the deflection angle range from −15 degrees to +15 degrees. Additionally, a free-running test of an underwater vehicle with six degrees of freedom based on a CFD method has been implemented by Kim et al. [10]. Straight line and steady turn maneuvering of the vehicle was also performed. The results showed that the maneuvering characteristics of the vehicle were in good agreement with the experimental results. An Autonomous Underwater Vehicle (AUV) with X-rudder plane configuration has been presented by Zhang et al. [11]. They predicted the hydrodynamic forces and moments of the X-rudder plane, and compared them with the results under the Cross-rudder plane configuration. An X-rudder configuration for an autonomous underwater vehicle has been tested by Zang et al. [12], and the hydrodynamic characteristics of the body and rudders were then introduced into the equation of motion and control of the vehicle. The maneuvering behaviors of a model of the CRN-INSEAN 2475 submarine with X-rudder or C-rudder configurations were predicted by Broglia et al. [13]. The trajectory parameters of turning motion for the submarine were predicted under angle of attacks of 5, 10, and 15 degrees. It was shown that the turning characteristics under the flapped X-rudder configuration

were better than the turning behavior of the submarine when using conventional X-plane rudder configurations. Captive model tests of the DARPA, SWE, and SMG submarines have been carried out by Piaggio et al. [14], in order to predict hull and rudder forces for the prediction of maneuvering characteristics. The failure of stern steering of the submarine with X-rudder plane or Cross-rudder plane configurations was also investigated. Hydrodynamic forces and moments of an underwater vehicle with Cross-rudder plane configuration were obtained through CFD-based simulation of rotating arm test, drift test, rudder test, and combination tests (between rotating arm and rudder deflection or drift–rudder) [15]. The obtained hydrodynamic coefficients were then introduced into the equations of turning motion to evaluate the turning behavior of the vehicle. The propeller thrust and resistance of the submarine obtained from the virtual self-propulsion test were compared to determine the rotational speed of the propeller [16]. Furthermore, visualization of the unsteady fluid flow surrounding the submarine with the propeller and Cross-rudder plane configuration was investigated. The turning ability of a submarine with the X-rudder plane configuration and virtual propeller has been predicted through numerical simulation of turning circles with different deflection of the rudders in Star-CMM+ code in [17]. The complex fluid flow around the DARPA SUBOFF submarine with rudder deflection has been analyzed based on OpenFOAM [18], where the hydrodynamic forces and moments of the rudder with a wide range of deflection angles were calculated and compared with experimental data. The forward running of a submarine near the free water surface has been simulated using Ansys Fluent code to predict the resistance of the hull under the Cross-rudder plane configuration, as well as the thrust and torque of the propeller [19]. The obtained results showed that the resistance of the hull and rudder plane near the free surface were increased by 129–174%, in comparison with the resistance of the submarine under deep water conditions.

It can be seen that the previous studies have focused on the maneuvering of submarines under a single stern rudder plane configuration, while few studies have analyzed the hydrodynamic characteristics of multiple types of rudder plane configuration. Therefore, three types of rudder configuration for the stern of a submarine are analyzed using Ansys Fluent code in this study in order to predict the hydrodynamic characteristics. The advantages of each stern rudder plane configuration in terms of submarine control will be evaluated. The geometry of the submarine with different stern rudder configurations in the fluid domain is generated using the Ansys Design Modeler. The fluid domain and the submarine's surface are then introduced for Ansys meshing, in order to discretize them into finite volume elements. Numerical simulation in Ansys Fluent using the generated meshes is then carried out to obtain the hydrodynamic forces and moments acting on the X-plane, Y-plane, and Cross-plane rudder configurations. Hydrodynamic coefficients of the stern rudder plane configurations are estimated through Taylor expansion of the deflection of the control surface. Finally, the best stern-plane rudder configuration, from the point of view of the submarine's maneuvering characteristics, will be analyzed.

2. Methodology

2.1. Coordinate Systems and Symbols

To predict the behaviors of the submarine, body-fixed ($Oxyz$) and earth-fixed ($O_1x_0y_0z_0$) coordinate systems are used to represent the dynamic behavior of the vehicle and its trajectory. The origin of the body-fixed coordinate system is located at the center of the midsection of the submarine. Figure 1 illustrates the two coordinate systems and definitions of the kinematics, forces, and moments of the submarine, in which u, v, and w stand for linear velocities along the x-, y-, and z-axes, while p, q, and r are angular velocities about these axes, respectively. Furthermore, X, Y, and Z indicate external forces of the submarine along the x-, y-, and z-axes and K, M, and N are the moments of the body about x-, y-, and z-axes, correspondingly.

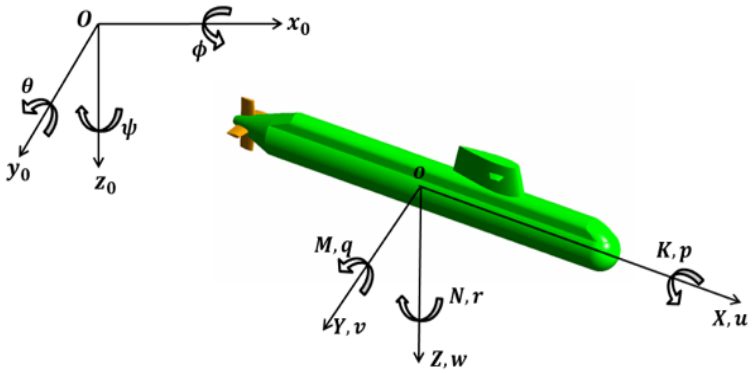

Figure 1. Coordinate systems and symbols.

2.2. Equation of Motion of the Submarine

Considering the motion of the submarine with six degrees of freedom, the equations for the submarine's motion in calm water in the body-fixed coordinate system have been described by Fossen [20], as follows:

$$m\left[\dot{u} - vr + wq - x_G\left(q^2 + r^2\right) + y_G(pq - \dot{r}) + z_G(pr + \dot{q})\right] = X \tag{1}$$

$$m\left[\dot{v} - wp + ur - y_G\left(r^2 + p^2\right) + z_G(qr - \dot{p}) + x_G(qp + \dot{r})\right] = Y \tag{2}$$

$$m\left[\dot{w} - uq + vp - z_G\left(p^2 + q^2\right) + x_G(rp - \dot{q}) + y_G(rq - \dot{p})\right] = Z \tag{3}$$

$$\begin{array}{c} I_x\dot{p} + (I_z - I_y)qr - I_{xz}(\dot{r} + pq) + I_{yz}(r^2 - q^2) + I_{xy}(qp - \dot{q}) \\ +m\left[y_G(\dot{w} - uq + vp) - z_G(\dot{v} - wp + ur)\right] = K \end{array} \tag{4}$$

$$\begin{array}{c} I_y\dot{q} + (I_x - I_z)rp - I_{xy}(\dot{p} + qr) + I_{zx}(q^2 - p^2) + I_{yz}(qp - \dot{r}) \\ +m\left[z_G(\dot{u} - vr + wq) - x_G(\dot{w} - uq + vp)\right] = M \end{array} \tag{5}$$

$$\begin{array}{c} I_z\dot{r} + (I_y - I_x)pq - I_{yz}(\dot{q} + rp) + I_{xy}(q^2 - p^2) + I_{zx}(rq - \dot{p}) \\ +m\left[x_G(\dot{v} - wp + ur) - y_G(\dot{u} - vr + wq)\right] = N \end{array} \tag{6}$$

where x_G, y_G, and z_G indicate the coordinate of center of gravity along the *x*-, *y*-, and *z*-axes, respectively; I_x, I_y, and I_z are mass moments of inertia of the ship about the *x*-, *y*-, and *z*-axes, respectively; I_{xy}, I_{yz}, and I_{zx} are the products of inertia about the *xy*-, *yz*- and *zx*-axes, respectively; and m is the mass of the ship.

Regarding the submarine's motion in calm water, the external force and moment in the right side of the equations can be divided into hull forces (F_H), propeller forces (F_P), and control forces (F_C). To steer the submarine with six degrees of freedom, the control force and moment of the rudders and stabilizers should be determined. These are then converted to a corresponding dimensionless form through dividing by (½ρV^{2}L^2) and (½ρV^{2}L^3), where L and V are the overall length and speed of the submarine, respectively, and ρ is the density of water. The hydrodynamic coefficients of the control plane are then obtained from the Taylor expansion, as shown in following equations.

$$F(X, Y, Z, K, M, N) = F_H + F_P + F_C \tag{7}$$

$$X'_C = X'_{\delta_r\delta_r}\delta_r^2 + X'_{\delta_s\delta_s}\delta_s^2 \tag{8}$$

$$Y'_C = Y'_{\delta_r}\delta_r + Y'_{\delta_r|\delta_r|}\delta_r|\delta_r| \tag{9}$$

$$Z'_C = Z'_{\delta_s}\delta_s + Z'_{\delta_s|\delta_s|}\delta_s|\delta_s| \tag{10}$$

$$K'_C = K'_{\delta_r}\delta_r + K'_{\delta_{r|\delta_r|}}\delta_r|\delta_r| \tag{11}$$

$$M'_C = M'_{\delta_s}\delta_s + M'_{\delta_s|\delta_s|}\delta_s|\delta_s| \tag{12}$$

$$N'_C = N'_{\delta_r}\delta_r + N'_{\delta_{r|\delta_r|}}\delta_r|\delta_r| \tag{13}$$

where the symbols on the right side of the equations are the hydrodynamic coefficients of the stern rudder plane configurations.

2.3. Simulation Method

The Reynolds-Averaged Navier–Stokes (RANS) method is used to analyze the fluid flow over the submarine in this study. Following this method, the instantaneous velocity is decomposed into its time-averaged velocity ($\overline{u}$) and fluctuating velocity, in which the fluctuating velocity is modeled as a function of the turbulence eddy viscosity and turbulence kinetic energy. The governing equations of the RANS method for incompressible flow have been introduced by Menter [21] and Wilcox [22], as follows:

$$\frac{\partial \overline{u}_i}{\partial x_i} = 0 \tag{14}$$

$$\frac{\partial \overline{u}_i}{\partial t} + \overline{u}_j\frac{\partial \overline{u}_i}{\partial x_j} = -\frac{\partial \overline{p}}{\partial x_i} + \nu\frac{\partial^2 \overline{u}_i}{\partial x_j \partial x_j} - \frac{\partial \tau_{ij}}{\partial x_j} \tag{15}$$

The Reynolds stress, $\tau_{ij} = \overline{u'_i u'_j}$, is modeled as the function of the eddy viscosity and kinetic energy based on the Boussinesq hypothesis. The turbulent model, *k-w* SST (Shear Stress Transport) [21], for solving turbulent flow around the submarine is presented as follows:

$$\frac{\partial k}{\partial t} + \overline{u}_i\frac{\partial k}{\partial x_i} = P_k - \beta^*\omega k + \frac{\partial}{\partial x_j}\left((v + \sigma_k v_t)\frac{\partial k}{\partial x_i}\right) \tag{16}$$

$$\frac{\partial \omega}{\partial t} + \overline{u}_i\frac{\partial \omega}{\partial x_i} = \frac{\gamma}{\mu_t}P_k - \beta\omega^2 + \frac{\partial}{\partial x_j}\left[(v + \sigma_\omega v_t)\frac{\partial \omega}{\partial x_i}\right] + 2(1 - F_1)\frac{\sigma_{\omega 2}}{\omega}\frac{\partial k}{\partial x_i}\frac{\partial \omega}{\partial x_i} \tag{17}$$

$$\mu_t = \frac{\rho a_1 k}{max(a_1\omega, \Omega F_2)} \tag{18}$$

where P_k is the production rate of turbulent kinetic energy by the mean flow. The variables are defined as follows.

$$P_k = \tau_{ij}\frac{\partial u_i}{\partial x_j}$$

$$\tau_{ij} = \mu_t\left(2S_{ij} - \frac{2}{3}\frac{\partial u_k}{\partial x_k}\delta_{ij}\right) - \frac{2}{3}\rho k\delta_{ij}$$

$$S_{ij} = \frac{1}{2}\left(\frac{\partial u_i}{\partial x_j} + \frac{\partial u_j}{\partial x_i}\right)$$

$$\beta_i = F_1\beta_{i,1} + (1 - F_1)\beta_{i,2}$$

$$\sigma_k = \frac{1}{F_1/\sigma_{k,1} + (1 - F_1)\sigma_{k,2}}$$

$$\sigma_\omega = \frac{1}{F_1/\sigma_{\omega,1} + (1 - F_1)\sigma_{\omega,2}}$$

$$F_1 = \tanh\left(\arg_1^4\right)$$

$$F_2 = \tanh\left(\arg_2^2\right)$$

$$arg_1 = min\left[max\left(\frac{\sqrt{k}}{\beta^*\omega y}; \frac{500\nu}{y^2\omega}\right), \frac{4\rho\sigma_{\omega_2}k}{CD_{k\omega}y^2}\right]$$

$$arg_2 = max\left(2\frac{\sqrt{k}}{0.09\omega y}; \frac{500\nu}{y^2\omega}\right)$$

$$CD_{k\omega} = max\left(2\rho\sigma_{\omega,2}\frac{1}{\omega}\frac{\partial k}{\partial x_i}\frac{\partial \omega}{\partial x_i}, 10^{-20}\right)$$

with the model constants $\sigma_{k,1}$ = 1.176, $\sigma_{\omega,1}$ = 2.0, $\sigma_{k,2}$ = 1.0, $\sigma_{\omega,2}$ = 1.168, a_1 = 0.31, $\beta_{i,1}$ = 0.075, and $\beta_{i,2}$ = 0.0828 [23].

3. Numerical Modeling

3.1. Case Study

A full-scale submarine was chosen as a target body in this study. Three stern-rudder plane configurations, including Cross-plane rudders, X-plane rudders, and Y-plane rudders, with the same span of 7.4 m were considered. The stern-rudder plane configurations were created from the NACA0020 profile. Figure 2 presents the geometry and main dimensions of the rudder plane configurations and the submarine. The definitions of hydrodynamic forces and moments acting on the Cross-rudder plane, X-rudder plane, and Y-rudder plane configurations are shown in Figure 3. The two opposite blades in the X-rudder plane and Cross-rudder plane configurations are all deflected about the same rotational axis, and are parallel and 0.578 m from the leading edge. Meanwhile, a pair of blades in the Y-rudder plane configuration are rotated about the rotational axes with the same distance from the leading edge but in different directions. The rudder deflection, δ_r, is defined for each type of the rudder plane configuration, as shown in Equations (19)–(21). Furthermore, the angle of deflection of each stabilizer, δ_s, is described in the left-hand equations. The hydrodynamic forces acting on each rudder plane configuration are defined in Figure 3.

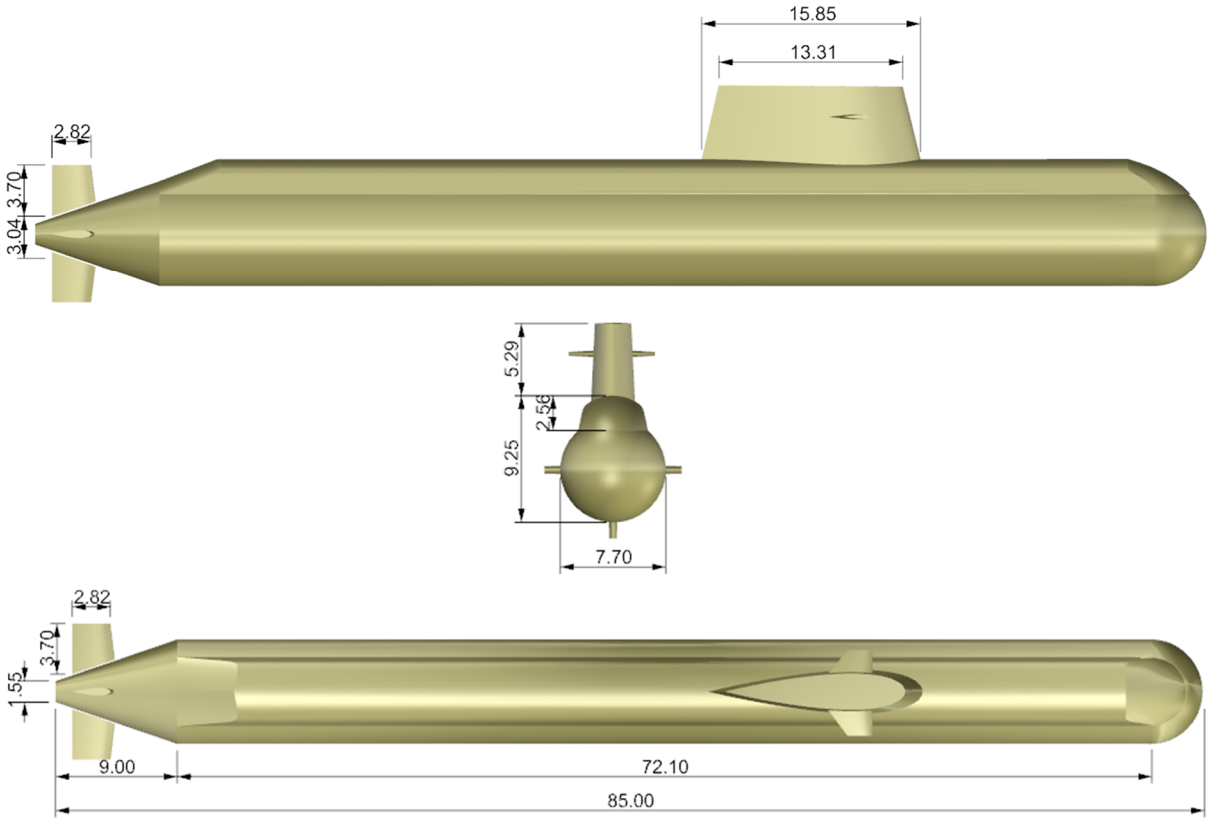

Figure 2. Main dimensions of the stern rudder configurations (in meters).

$$\delta_{r\_Cross} = \frac{(\delta_2 + \delta_4)}{2} \quad (19)$$

$$\delta_{r\_X} = \frac{(\delta_1 + \delta_2 + \delta_3 + \delta_4)}{4} \tag{20}$$

$$\delta_{r\_Y} = \frac{\delta_1 + \delta_2 + \delta_3}{3} \tag{21}$$

$$\delta_{s\_Cross} = \frac{(-\delta_1 - \delta_3)}{2} \tag{22}$$

$$\delta_{s\_X} = \frac{(-\delta_1 + \delta_2 - \delta_3 + \delta_4)}{4} \tag{23}$$

$$\delta_{s\_Y} = \frac{(\delta_2 - \delta_3)}{2} \tag{24}$$

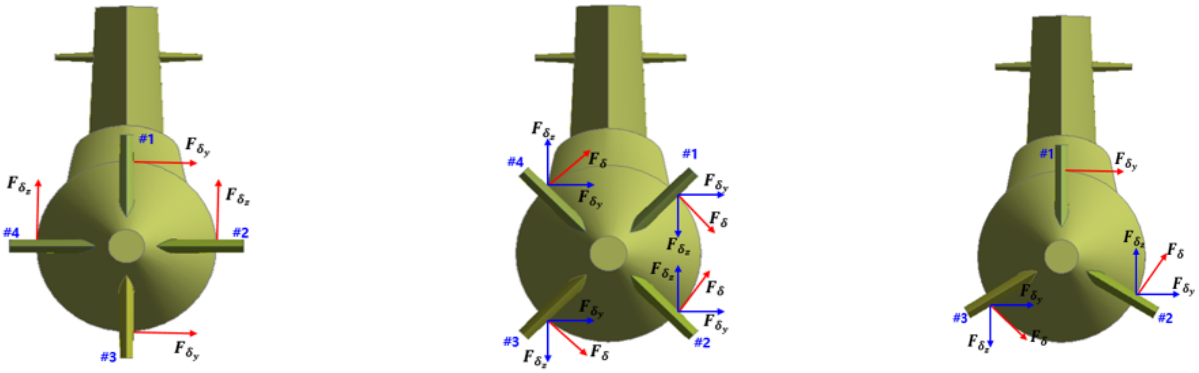

Figure 3. Definitions of the (**a**) Cross-rudder plane, (**b**) X-rudder plane, and (**c**) Y-rudder plane configurations, including their hydrodynamic forces and moments.

3.2. CFD-Based Modeling

A rectangular shape was selected as a fluid domain for simulating fluid flow over the submarine without the effect of reverse flow. Following the ITTC Recommendation [24], a rectangular domain of 7L in length, 4L in breadth, and 3L in height was created, where L stands for the whole length of the submarine. The distance from the bow of the submarine to the front surface of the fluid domain was set as 2L, and the submarine was located in the middle of the fluid domain. In addition, physical conditions should be applied to the outer surfaces of the fluid domain. The submarine speed was assigned for the front surface as the velocity inlet, while the pressure-outlet condition was applied for the back surface. Symmetric conditions were set for the side, top, and bottom surfaces. The no-slip wall condition was set on the surfaces of the submarine hull and control surfaces. Figure 4 presents the fluid domain and the boundary conditions on the submarine and outer surfaces.

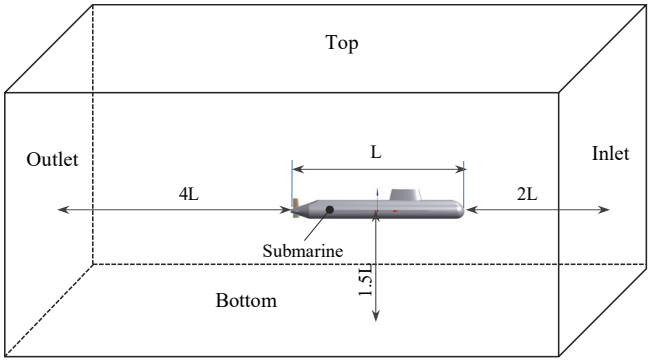

Figure 4. Fluid domain and boundary conditions.

To prepare for the simulation, the fluid domain was discretized using tetrahedral elements, as shown in Figure 5. The boundary layer of fluid flow surrounding the submarine was modeled using layers of prism elements. The first layer thickness was determined from the dimensionless wall distance (y+ value). With a submarine speed of 20 knots, the Reynolds number was 1.0×10^9 and the regime of fluid flow over the submarine and control surfaces was full turbulence. According to Oh et al. [25], the value of y+ is given about 3000–5000 for Re = 1.0×10^9. Therefore, the value of y+ was chosen as 3000, and the height of the first layer thicknesses on the hull and the stern rudder plane configuration was then calculated as 9.0 mm.

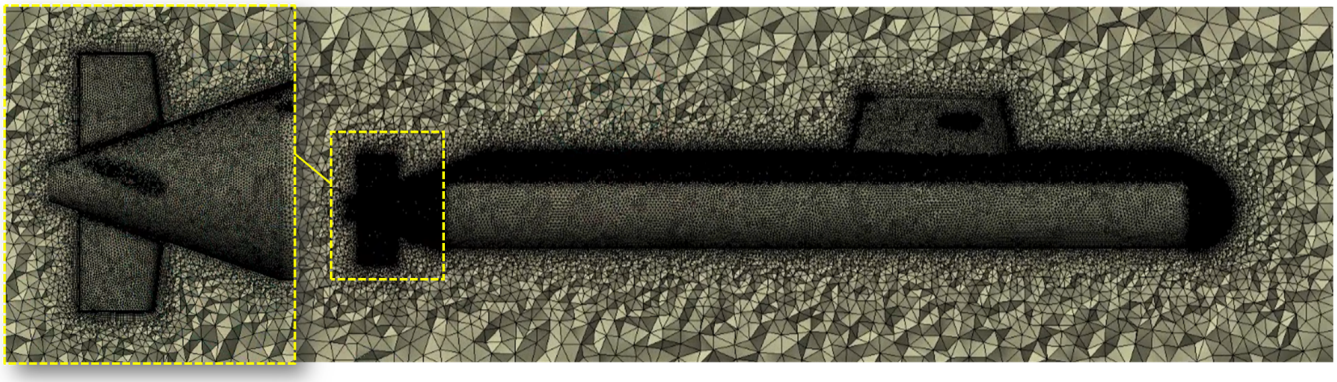

Figure 5. Local mesh in stern area and local mesh around the submarine.

The incompressible RANS solver in Ansys Fluent was used to simulate fluid flow through the submarine with the three rudder plane configurations. According to the ITTC recommendation [24], the two-equation models of turbulence model, turbulence model of k-ε realizable, or turbulence model of k-ω SST (Shear Stress Transport) are recommended for simulating turbulent flow around a submarine in motion. Thus, the k-ω SST turbulence model was selected for modeling turbulent fluid flow around the submarine. The pressure field was obtained by solving the momentum equation using the SIMPLE (Semi-Implicit Pressure Link Equation) algorithm. The second-order upwind method was employed to estimate the face values through interpolation of cell center values and pressure values.

4. Results

To verify the simulation results, the force along the y-axis and moment about the z-axis under the X-rudder plane configuration obtained from the CFD-based simulation in Ansys Fluent were compared with the corresponding force and moment of a similar model (SWE submarine), which was previously estimated by Piaggio et al. [14], as shown in Figure 6. It can be seen that the obtained results were consistent with the experimental results [9]. The difference between the hydrodynamic coefficients of the X-rudder plane configuration and the previous results may have resulted from the ignorance of strong turbulent flow induced by the rudders, stabilizers, and the submarine's body, as the fluid flow through the stern rudder plane configuration on the submarine is simulated in steady state. The comparison between the current and previous results is detailed in Table 1. Next, the numerical simulation setup was applied to estimate the hydrodynamic forces and moments of the rudder plane configuration.

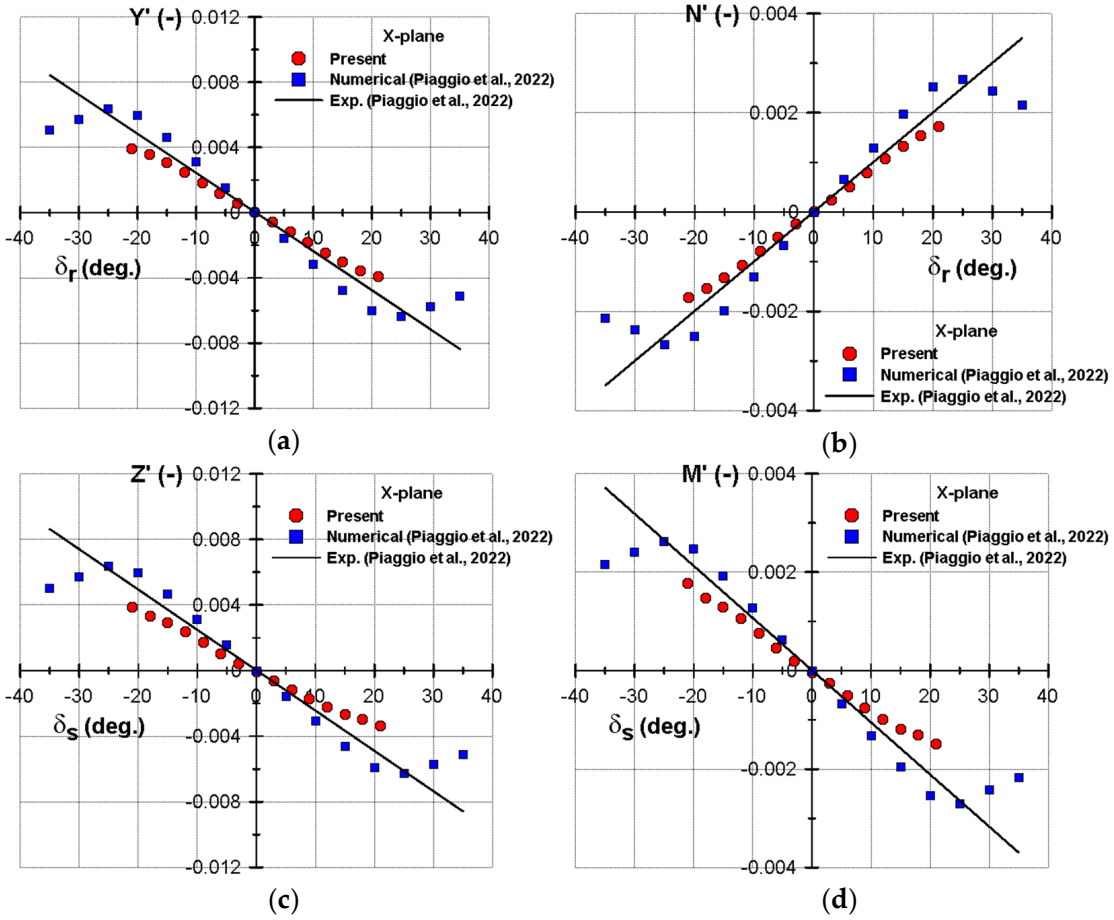

Figure 6. Comparison between current results and the previous results for rudders and stabilizers on am SWE submarine in Piaggio et al., 2022 [14]. (**a**) Y−force of rudders versus angle of attack of the rudder, (**b**) Y−force of rudders versus angle of attack of the rudders, (**c**) Y−force of stabilizers versus angle of attack of the stabilizers, (**d**) Y−force of stabilizers versus angle of attack of the stabilizers.

Table 1. Comparison of the linear coefficients of the X-rudder plane configuration between current study and the experimental study of Piaggio [14].

Symbol	Current Study	Experiment (Piaggio et al. [14])	Difference (%)
Y'_{δ_r}	1.17×10^{-2}	1.38×10^{-2}	15.22
Z'_{δ_s}	1.12×10^{-2}	1.41×10^{-2}	20.57
M'_{δ_s}	4.84×10^{-3}	6.10×10^{-3}	20.66
N'_{δ_r}	-5.05×10^{-3}	-5.70×10^{-3}	11.4

To predict the hydrodynamic forces and moments acting on the rudders and stabilizers, the submarine was forced to run steadily at a speed of 20 knots with different angles of the rudder and stabilizer. Both the rudder and stabilizer were rotated from 0 to 21 degrees about the z-axis and y-axis, respectively. The interval of the deflected angle for the simulation was 3 degrees for each of the cases. As the submarine has a symmetrical body, the rudders were rotated in one direction and the obtained results are presented in both rotating directions. However, it was necessary to rotate the stabilizers in both directions about the axis of rotation. The hydrodynamic forces and moments acting on each rudder-plane were estimated in the numerical simulation. Figure 7 presents the results of hydrodynamic forces and moments acting on the X-rudder plane, Y-rudder plane, and Cross-rudder plane configurations obtained from the CFD-based simulation. It can be seen that the forces

and moments increased as the deflection angle of the rudder and stabilizer increased. The hydrodynamic forces along the x- and y-axes of the X-rudder plane were larger than the corresponding forces acting on the Cross-rudder plane and Y-rudder plane. The roll moment of the X-rudder plane was rather small, in comparison with the moment acting on the left rudder plane configurations. This can be explained by the symmetric arrangement of the X-rudder configuration, which induces the small value in hydrodynamic force along the z-axis as well as the roll moment. A similar trend can be found in the hydrodynamic force along the z-axis and the moment about the y-axis of the stabilizers, as shown in Figure 8. The force along the x-axis and the moment about the y-axis of the stabilizers in the X-rudder plane configuration were significantly larger than the force and moment of stabilizers in the Cross-rudder plane or Y-rudder plane configurations. On the other hand, the hydrodynamic force along the z-axis and the moment about the y-axis in the Cross-rudder plane configuration were slightly smaller than the corresponding force and moment of the Y-rudder plane configuration when the stabilizers were turned down, while a discrepancy between the hydrodynamic forces of these two rudder plane configurations was found in the positive deflection angle range.

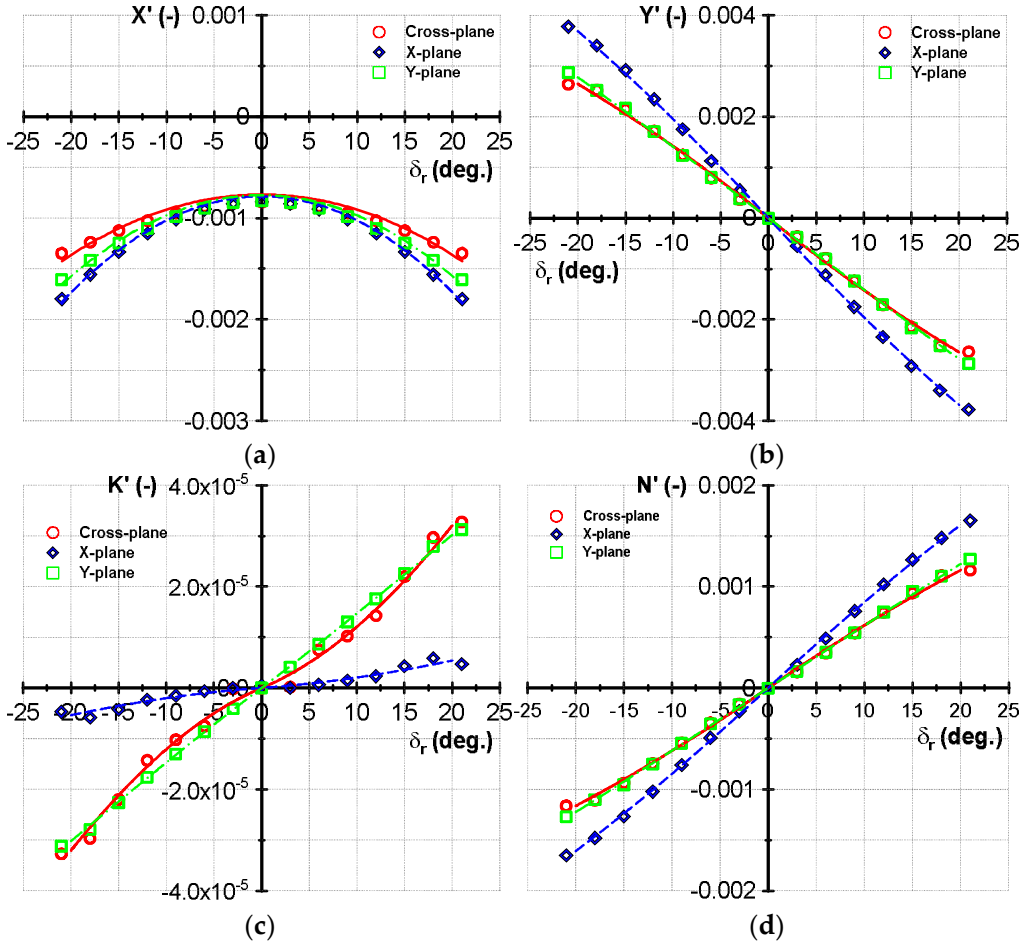

Figure 7. Hydrodynamic forces and moments of the rudders in horizontal plane. (**a**) Rudder force along x-axis, (**b**) Rudder force along y-axis, (**c**) Rudder moment about x-axis, (**d**) Rudder moment about z-axis.

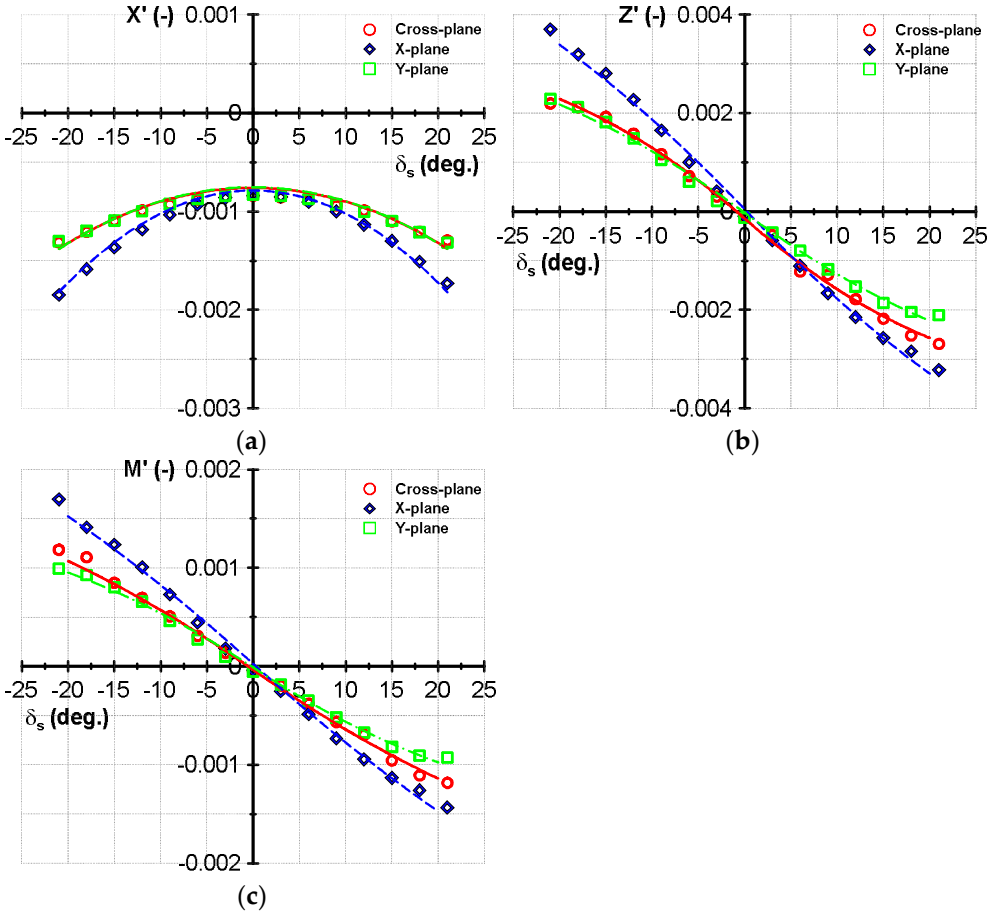

Figure 8. Hydrodynamic forces and moments of the stabilizers in vertical plane. (**a**) X-force of the stabilizers, (**b**) Z-force of the stabilizers, (**c**) Stabilizer moment about *y*-axis.

The variation of hydrodynamic forces and moments under the stern rudder plane configurations were then fitted using the least squares method, in order to estimate the hydrodynamic coefficients of the rudders and stabilizers. Table 2 depicts the hydrodynamic coefficients under the three stern-rudder plane configurations. The first-order derivative of the force along the *y*-axis of the X-rudder plane configuration was about 1.36 times and 1.45 times greater than that of the corresponding force acting on the Cross-rudder plane and Y-rudder plane configurations, respectively. The first-order derivative of the force along the *z*-axis of the X-rudder plane configuration was about 1.18 and 1.41 times greater than those of the Cross-rudder plane and Y-rudder plane, respectively. Furthermore, the second-order derivative of the rudder's force along the *x*-axis of the X-rudder plane configuration was about 1.67 times larger than that of the Cross-rudder plane configuration, but was approximately the same as that along the *x*-axis of the Y-rudder plane configuration. On the other hand, the first-order coefficients of the roll moment of the X-rudder plane were very small in comparison with the roll moment of the left rudder plane configurations.

Table 2. Hydrodynamic coefficients under the Cross-rudder plane, X-rudder plane, and Y-rudder plane configurations.

Symbol	Cross-Rudder Plane	X-Rudder Plane	Y-Rudder Plane
$X'_{\delta_r\delta_r}$	-5.27×10^{-3}	-8.81×10^{-3}	-9.06×10^{-3}
$X'_{\delta_s\delta_s}$	-4.91×10^{-3}	-9.66×10^{-3}	-7.40×10^{-3}
Y'_{δ_r}	8.62×10^{-3}	1.17×10^{-2}	8.07×10^{-3}
$Y'_{\delta_r\lvert\delta_r\rvert}$	-2.57×10^{-3}	-2.74×10^{-3}	-1.60×10^{-4}

Table 2. *Cont.*

Symbol	Cross-Rudder Plane	X-Rudder Plane	Y-Rudder Plane
Z'_{δ_s}	9.48×10^{-3}	1.12×10^{-2}	7.95×10^{-3}
$Z'_{\delta_s\|\delta_s\|}$	-6.97×10^{-3}	-4.28×10^{-3}	-4.47×10^{-3}
K'_{δ_r}	-4.48×10^{-5}	-7.61×10^{-6}	-8.11×10^{-5}
$K'_{\delta_r\|\delta_r\|}$	-1.43×10^{-4}	-2.38×10^{-5}	-2.11×10^{-5}
M'_{δ_s}	3.76×10^{-3}	4.84×10^{-3}	3.54×10^{-3}
$M'_{\delta_s\|\delta_s\|}$	-1.54×10^{-3}	-1.35×10^{-3}	-2.11×10^{-3}
N'_{δ_r}	-3.73×10^{-3}	-5.05×10^{-3}	-3.52×10^{-3}
$N'_{\delta_r\|\delta_r\|}$	9.67×10^{-4}	1.03×10^{-3}	-1.71×10^{-4}

Local views of the pressure distribution on the rudder plane configurations are shown in Figures 9–11 for the static rudder test and static stabilizer test at a deflection angle of 15 degrees. It can be observed that the static pressure distributions were asymmetric on the deflected blades under the Cross-rudder plane configuration. A stagnation region surrounding the leading edge of the left blades of the rudder plane configuration can be seen. However, the asymmetric pressure field on all blades in the X-rudder plane and the two inclined blades in the Y-rudder plane configurations for any deflection angle can be observed.

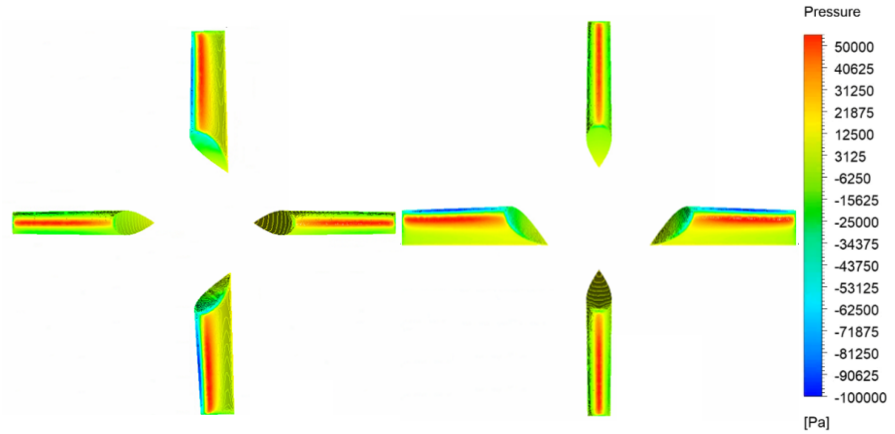

(**a**) (**b**)

Figure 9. Static pressure contour on the Cross-plane rudder configuration at an angle of deflection of 15 degrees: (**a**) deflection of rudders; (**b**) deflection of stabilizers.

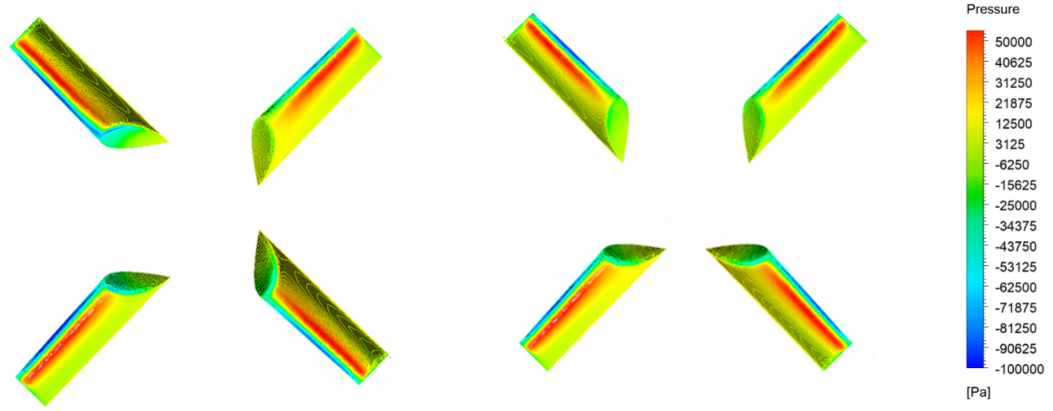

(**a**) (**b**)

Figure 10. Static pressure contour on the X-rudder plane configuration at an angle of deflection of 15 degrees: (**a**) deflection of rudders; (**b**) deflection of stabilizers.

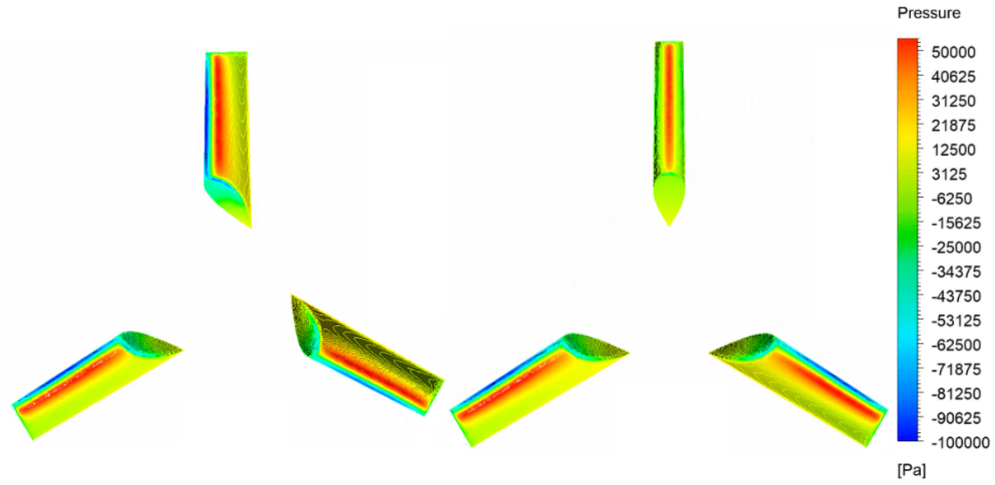

(**a**) (**b**)

Figure 11. Static pressure contour on the Y-rudder plane configurations at an angle of deflection of 15 degrees: (**a**) deflection of rudders; (**b**) deflection of stabilizers.

5. Conclusions

In this study, numerical studies focused on the stern rudder plane configurations of a submarine submerged in deep water were performed using RANS-based simulation. Deflection angles ranging from −21 degrees to +21 degrees were considered, allowing for comparison of the hydrodynamic forces and moments of the rudders and stabilizers at different deflection angles.

The variation in the hydrodynamic forces and moments about the *x*-, *y*-, and *z*-axes under the Cross-rudder plane, X-rudder plane, and Y-rudder plane configurations with the same span were predicted. The hydrodynamic coefficients of the rudders and stabilizers were then obtained through Taylor expansion of the hydrodynamic forces and moments. It was proved that the hydrodynamic forces of the X-rudder plane configuration are the largest, in comparison with the forces acting on the left cases (excluding the roll moment). The numerical analysis indicated that the first-order derivative of the Y-force for the X-rudder plane configuration exhibited a significantly higher magnitude, being approximately 1.36 and 1.45 times greater than those observed under the Cross-rudder and Y-rudder plane configurations, respectively. Furthermore, the first-order derivative of the Z-force associated with the X-rudder plane configuration also surpassed those of the Cross-rudder and Y-rudder plane configurations, being approximately 1.18 and 1.41 greater, respectively. The hydrodynamic force along the *z*-axis and the moment about the *y*-axis of the stabilizers in the Cross-rudder plane configuration were considerably larger than the corresponding force and moment under the Y-rudder plane configuration for positive deflection angles.

The hydrodynamic forces and moments of the stern rudder plane configurations were assessed according to RANS-based simulation in steady state. In addition, fluid flow through the rudder and stabilizer at high deflection angles was not investigated. Therefore, CFD-based estimation of the hydrodynamic coefficients of the stern rudder plane configuration under unsteady fluid flow conditions should be assessed in further research.

Author Contributions: Conceptualization and methodology, T.T.N.; resources, T.L.M.; software, T.L.P., T.T.N. and T.L.M.; data analysis and validation, T.L.P. and T.T.N.; writing-original draft preparation, T.L.P. and T.T.N.; writing-review and editing, T.L.P., T.T.N. and T.L.M.; Funding acquisition, T.T.N. All authors have read and agreed to the published version of the manuscript.

Funding: This research is funded by Funds for Science and Technology Development of the University of Danang under project number B2020-DN02-85.

Institutional Review Board Statement: Not applicable.

Informed Consent Statement: Not applicable.

Data Availability Statement: The data presented in this study are available on request from the corresponding author.

Conflicts of Interest: The authors declare no conflicts of interest.

References

1. Park, J.Y.; Kim, N.; Shin, Y.K. Experimental study on hydrodynamic coefficients for high-incidence-angle maneuver of a submarine. *Int. J. Nav. Archit. Ocean Eng.* **2016**, *9*, 100–113. [CrossRef]
2. Ke, L.; Ye, J.; Liang, Q. Experimental Study on the Flow Field, Force, and Moment Measurements of Submarines with Different Stern Control Surfaces. *J. Mar. Sci. Eng.* **2023**, *11*, 2091. [CrossRef]
3. Kim, H.; Hong, S.K. Numerical study on the hydrodynamic control derivatives of a high-speed underwater vehicle with X-stern configuration. *J. Mech. Sci. Technol.* **2012**, *25*, 3075–3082. [CrossRef]
4. Fureby, C.; Anderson, B.; Clarke, D.; Erm, L.; Henbest, S.; Giacobello, M.; Jones, D.; Nguyen, M.; Johansson, M.; Jones, M.; et al. Experimental and numerical study of a generic conventional submarine at 10° yaw. *Ocean Eng.* **2016**, *116*, 1–20. [CrossRef]
5. Khan, M.K.; Korulla, M.; Nagarajan, V.; Sha, O.P. Steady velocity measurements in the stern wake of submarine hull form at high angles of incidence. *Ocean Eng.* **2023**, *277*, 114281. [CrossRef]
6. Nguyen, T.T.; Yoon, H.K.; Park, Y.; Park, C. Estimation of hydrodynamic derivatives of full-scale submarine using RANS solver. *J. Ocean Eng. Technol.* **2018**, *20*, 386–392. [CrossRef]
7. Cho, Y.J.; Seok, W.; Cheon, H.H.; Rhee, S.H. Maneuvering simulation of an X-plane submarine using computation fluid dynamics. *Int. J. Nav. Archit. Ocean Eng.* **2020**, *12*, 843–855. [CrossRef]
8. Wu, S.J.; Lin, C.C.; Liu, T.L.; Su, I.H. Robust design on the arrangement of a sail and control planes for improvement of underwater vehicle's maneuverability. *Int. J. Nav. Archit. Ocean Eng.* **2020**, *12*, 617–635. [CrossRef]
9. Jeon, M.J.; Yoon, H.K.; Hwang, J.; Cho, H.J. Analysis of the dynamic characteristics for the change of design parameters of an underwater vehicle using sensitivity analysis. *Int. J. Nav. Archit. Ocean Eng.* **2018**, *10*, 508–519. [CrossRef]
10. Kim, H.; Ranmuthugala, D.; Leong, Z.Q.; Chin, C. Six-DOF simulation of an underwater vehicle undergoing straight line and steady turning maneuvers. *Ocean Eng.* **2018**, *150*, 102–112. [CrossRef]
11. Zhang, Y.; Li, Y.; Sun, Y.; Zeng, J.; Wan, L. Design and simulation of X-rudder AUV's motion control. *Ocean Eng.* **2017**, *137*, 204–214. [CrossRef]
12. Zhang, Y.; Li, Y.; Zhang, G.; Zeng, J.; Wan, L. Design of X-rudder autonomous underwater vehicle's quadruple-rudder allocation with Le'vy flight character. *Int. J. Adv. Robot. Syst.* **2017**, *14*, 1–15. [CrossRef]
13. Broglia, R.; Cannarozzo, M.; Dubbioso, G.; Zaghi, S. Free Running Prediction of a Fully Appended Submarine: Effects of Stern Plane Configurations. In Proceedings of the VI International Conference on Computational Methods in Marine Engineering, Rome, Italy, 15–17 June 2015.
14. Piaggio, B.; Vernengo, G.; Ferrando, M.; Mazzarello, G.; Viviani, M. Submarine Manoeuvrability Design: Traditional Cross-Plane vs. *x-Plane Configurations in Intact and Degraded Conditions. J. Mar. Sci. Eng.* **2022**, *10*, 2014.
15. Park, J.H.; Shin, M.S.; Jeon, Y.H.; Kim, Y.G. Simulation-Based Prediction of Steady Turning Ability of a Symmetrical Underwater Vehicle Considering Interactions Between Yaw Rate and Drift/Rudder Angle. *J. Ocean Eng. Technol.* **2021**, *35*, 99–112. [CrossRef]
16. Pan, Y.; Zhang, H.; Zhou, Q. Numerical simulation of unsteady propeller force for a submarine in straight ahead sailing and steady diving maneuver. *Int. J. Nav. Archit. Ocean Eng.* **2019**, *11*, 899–913. [CrossRef]
17. Han, K.; Cheng, X.; Liu, Z.; Huang, C.; Chang, H.; Yao, J.; Tan, K. Six-DOF CFD Simulations of Underwater Vehicle Operating Underwater Turning Maneuvers. *J. Mar. Sci. Eng.* **2021**, *9*, 1451. [CrossRef]
18. Guo, H.; Li, G.; Du, L. Investigation on the flow around a submarine under the rudder deflection condition by using URANS and DDES methods. *Appl. Ocean Res.* **2023**, *131*, 103448. [CrossRef]
19. Vali, A.; Saranjam, B.; Kamali, R. Experimental and Numerical Study of a Submarine and Propeller Behaviors in Submergence and Surface Conditions. *J. Appl. Fluid Mech.* **2018**, *11*, 1297–1308. [CrossRef]
20. Fossen, T.I. *Guidance and Control of Ocean Vehicles*, 3rd ed.; John Wiley and Son: Baffins Lane, UK, 1999; pp. 168–180.
21. Menter, F. Two-Equation Eddy-Viscosity Turbulence Models for Engineering Applications. *AIAA* **1994**, *32*, 1598–1605. [CrossRef]
22. Wilcox, C.D. *Turbulence Modeling for CFD*, 3rd ed.; DCW Industries Inc.: La Cafiada, CA, USA, 2006.
23. Ansys Inc. *Ansys Fluent Theory Guide 12.0*; Ansys Inc.: Canonsburg, PA, USA, 2012; pp. 64–65.

24. ITTC. Practical Guidelines for Ship CFD Application. In *Proceedings of the 26th International Towing Tanks Conference, Rio de Janeiro, Brazil, 28 August–3 September 2011*; Number 7.5-03-02-03; ITTC: Beijing, China, 2011. Available online: https://ittc.info/media/1357/75-03-02-03.pdf (accessed on 1 April 2024).
25. Oh, K.J.; Kang, S.H. Full scale Reynold number effects for the viscous flow around the ship stern. *Comput. Mech.* **1992**, *9*, 85–94. [CrossRef]